Met. Mater. Int., Vol. 19, No. 2 (2013), pp. 197~203
doi: 10.1007/s12540-013-2009-y

Transition of Crack Propagation from a Transgranular to an Intergranular Path in an Overaged Al-Zn-Mg-Cu Alloy During Cyclic Loading

Xu Chen[1,2], Zhiyi Liu[1,2,*], Peng Xia[1,2], Ailin Ning[3], and Sumin Zeng[1,2]

[1]Key Laboratory of Nonferrous Metal Materials Science and Engineering, Ministry of Education, Central South University, Changsha 410083, China
[2]School of Material Science and Engineering, Central South University, Changsha 410083, China
[3]Department of Mechanical Engineering, Shaoyang University, Shaoyang 422000, China

(received date: 21 November 2011 / accepted date: 20 May 2012)

The fatigue crack propagation behavior in the overaged Al-Zn-Mg-Cu alloy was characterized by optical microscopy, scanning electron microscopy, transmission electron microscopy and electron backscatter diffraction. The results revealed that a fatigue crack tended to transgranularly propagate in the near-threshold regime, whereas intergranular crack propagation was dominant at the high ΔK regime. The transition of crack propagation from a transgranular to an intergranular path that occurred in the Paris regime was strongly influenced by the misorientation of adjacent grains and precipitate free zones. In addition, a crystallographic model of crack propagation was proposed to interpret the transition. The fatigue short crack propagation on a single slip plane was responsible for the formation of a transgranular propagation path in the near-threshold regime. The fatigue long crack propagation, which was conducted by a duplex slip mechanism in the Paris regime, led to the formation of fatigue striations. The formation of a zigzag crack in the near-threshold regime was ascribed to the high misorientation of adjacent grains.

Key words: alloys, aging, fatigue, electron backscattering diffraction, scanning electron microscopy

1. INTRODUCTION

Al-Zn-Mg-Cu series alloys have been widely used for structural application in the aerospace industry due to the combinations of low density, high strength, excellent stress corrosion cracking resistance and superior fracture toughness [1,2]. With the rapid development of the aerospace industry, mechanical properties are required to be further improved to meet the demand of applications, especially fatigue. Fatigue fracture is believed to be one of the most dangerous forms of fracture owing to the fact that it occurs under loads much lower than those required producing failure by static loading.

Over the past several decades, studies have been focused on the research of fatigue crack initiation and crack propagation behavior in aluminum alloys, by means of optical microscopy [3,4], scanning electron microscope [5-7], transmission electron microscope [8], in situ high-resolution synchrotron X-ray microtomography [9] and electron backscatter diffraction [10]. Based on the research by Chan [11], competing fatigue mechanisms involving crack initiation at persistent slip bands, grain boundaries, pores and particles, have been reported to occur at surface sites in the high-cycle fatigue regime, but they shift to interior sites in the ultrahigh-cycle fatigue regime. Zheng *et al*. [7] revealed that cracks initiated at small pits on the sample surface, second particles such as the large Fe-bearing particles, and second phase particles/matrix interface at the early stage of a four-point-bend test in an AA2524 alloy.

A fundamental and effective model was well known to explain the crack propagation behavior proposed by Zhai *et al*. [5], and indicated that crack plane tilt and twist occurred because of a change of crystallographic orientation when the crack passed through a grain boundary. Apparently, this model explained that the crack completely crossed the grain boundary of adjacent grains. Jian *et al*. [10] investigated the crystallographic mechanism of long crack propagation in an overaged 7075 aluminum alloy, in which both intergranular and transgranular crack propagation were observed. However, the transition of crack propagation from a transgranular mode to an intergranular mode was not mentioned. In a 2024-T351 aluminum alloy, Hénaff *et al*. [12] revealed that intergranular crack propagation occurred in corrosion fatigue experiments. It should be noted that the fatigue experiments were carried out in a saline solution comprised of distilled

*Corresponding author: liuzhiyi@mail.csu.edu.cn

water with a 3.5% NaCl addition, and the crack propagation behavior was greatly influenced by the corrosive medium. Additionally, Forsyth [13] described the relation between short crack propagation and the applied stress direction by advancing two stages of short crack propagation. In Stage I the crack grows along the plane of maximum shear stress, and in Stage II the crack grows on the plane normal to the direction of maximum principle stress. Recently, Künkler *et al.* [14] showed that the transition of short crack propagation from Stage I to Stage II was accompanied by a noticeable change from a single slip mechanism to a multiple slip mechanism. So far, no previous work has been conducted to report the transition of crack propagation path for an overaged Al-Zn-Mg-Cu alloy during cyclic loading.

In this study, therefore, we analyzed fatigue crack propagation behavior in the overaged Al-Zn-Mg-Cu alloy. The transition of crack propagation from a transgranular to an intergranular path is also described in detail.

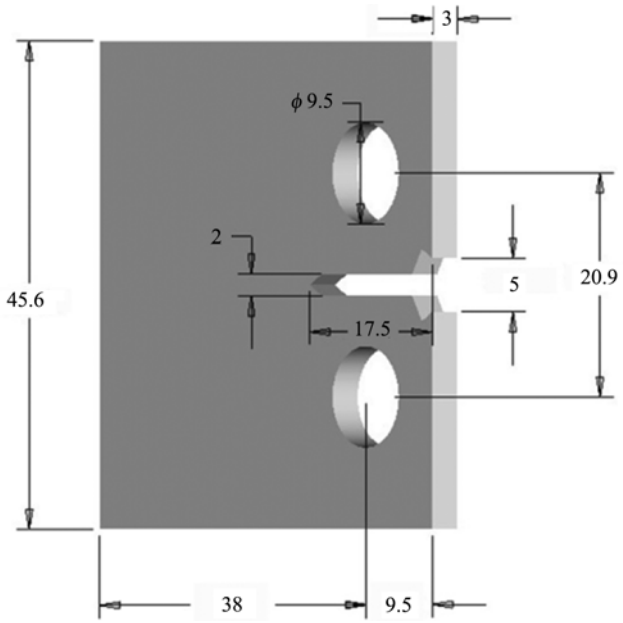

Fig. 1. Compact tension specimen geometry of the fatigue crack propagation studies (mm).

2. EXPERIMENTAL PROCEDURES

The received experimental material was an Al-Zn-Mg-Cu alloy sheet with a 3 mm thickness. Its chemical compositions (in weight percent) are listed in Table 1. The samples were solution-treated at 470 °C for 1 h, cold water quenched and immediately given a double-stage ageing treatment (aged at 125 °C for 3 h and then 170 °C for 10 h in air furnace) after pre-stretching.

A TecnaiG^{2}20 transmission electron microscopy (TEM) with an operating voltage of 200 kV, together with selected area electron diffraction (SAED) was used to characterize the microstructures of the overaged samples. Slices for the TEM test were cut directly from samples, and subsequently were ground to 100 μm and punched into a 3 mm disc. The electrolyte was a mixture of 70% methanol and 30% nitric acid, and thinning was performed at −25 °C. The tensile properties were evaluated with a CSS 44100 universal testing machine at room temperature in the long transverse (LT) direction with a 2 mm/min loading speed using 30 mm gauge length specimens.

A fatigue crack propagation (FCP) test was performed on compact tension (CT) specimens taken from the strips in the L-T orientation with a size of 45.6 mm × 38 mm × 3 mm (L×W×B) to obtain the FCP rates. FCP tests were conducted at a stress ratio ($R=K_{min}/K_{max}$) of 0.1 with a sine-wave loading frequency of 10 Hz on an MTS810 machine at room temperature in a laboratory air environment. The CT specimen geometry of the crack propagation is shown in Fig. 1. The fatigue fracture surfaces were analyzed by a FEI Quanta 200 scanning electron microscope (SEM) with an operating voltage of 15 kV. The fracture surfaces were rinsed by acetone prior to the SEM observations.

Fatigued samples were unloaded in the near-threshold regime, Paris regime and high ΔK regime, respectively, to detect the crack propagation paths and the misorientation distributions of grains along the fatigue crack by the electron backscatter diffraction (EBSD) method. The preparation of samples for EBSD studies consisted of conventional mechanical grinding followed by electropolishing which was carried out on DC stabilized power supply. The samples were electropolished in a solution consisting of 10% perchloric acid and 90% ethanol at 18-23 V for 10-20 s. EBSD measurements were performed on a Sirion 200 field emission gun scanning electron microscope with an accelerating voltage of 20 kV. Moreover, the corresponding optical metallographic examination and SEM observation of the EBSD samples were also carried out to reveal the crack propagation paths.

Table 1. Chemical compositions of the studied Al-Zn-Mg-Cu alloy

(in wt%)

Alloy	Zn	Mg	Cu	Cr	Mn	Ti	Fe	Si	Al
Al-Zn-Mg-Cu alloy	5.50	2.30	1.50	0.21	0.04	0.03	0.03	0.03	Balance

3. RESULTS

3.1. Microstructures and properties

The typical microstructures of the overaged Al-Zn-Mg-Cu alloy are characterized in Fig. 2, and the corresponding room temperature tensile properties of the alloy are given in Table 2. The precipitates were distributed homogeneously in the aluminum matrix, as shown in Fig. 2(a). The selected area diffraction patterns (SADPs) in $<001>_{Al}$ projection are shown in Fig. 2(b) and indicate the notable presence of strong diffraction spots at 1/3 and 2/3 $\{220\}_{Al}$ associated with the formation of η' precipitates. The SADPs failed to reveal any particles that could be identified as GP zones, since GP zones tend to form at the early stages of ageing. Therefore, it is unlikely that there would be any at any later stage. Corresponding SADPs in Fig. 2(b) also do not reveal spots consistent with η phase, so it is reasonable to conclude that η' precipitates are the dominant precipitates in the overaged alloy. Fig. 2(c) shows that grain boundaries are decorated intermittently by equilibrium η precipitates. This is to be expected in general because the velocity of solute diffusivity is greater at grain boundaries than that in grain interiors, which allows more rapid growth of precipitates. The formation of grain boundary precipitates (GBPs) leads to the depletion of solute atoms and vacancies near the grain boundary and consequent formation of precipitate free zones (PFZs).

The variation of the crack propagation rate (da/dN) with a stress intensity factor range (ΔK) of the overaged Al-Zn-Mg-Cu alloy at R=0.1 and 10 Hz is revealed in Fig. 3, which suggest that the intermediate ΔK regime, known as the Paris regime, exhibits a linear variation of log da/dN with log ΔK.

3.2. Short crack propagation

It is generally accepted that fatigue crack initiation and crack propagation in the near-threshold regime are microstructure-sensitive [15]. To better understand the detail of short crack propagation, the misorientation distributions of grains near the fatigue crack were measured by an EBSD analysis accessory and the corresponding optical microstructure observation of the same crack was also carried out, as shown in Fig. 4. With continuing cyclic loading, the crack initiated on the surface layer starts to propagate into adjacent grains. In this work, the short crack presents a transgranular extension coupled with propagation in the straight-line path when the crack passes through grains A, B and C sequentially, as shown in Fig. 4(a). However, fatigue crack begins to deflect when it reaches the grain boundary between grain C and grain D, and similar crack deflection is also observed between grain D and grain E. The difference in color in Fig.

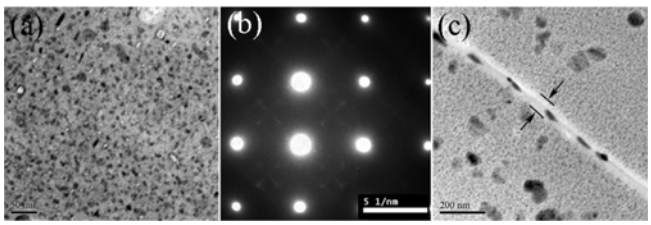

Fig. 2. Transmission electron micrograph of precipitates (a) and corresponding selected area diffraction patterns in $<001>_{Al}$ projection (b) coupled with the micrograph of grain boundary (c).

Table 2. Tensile properties of the overaged Al-Zn-Mg-Cu alloy at room temperature

Ultimate Strength (MPa)	Yield Strength (MPa)	Elongation (%)
498	430	12.1

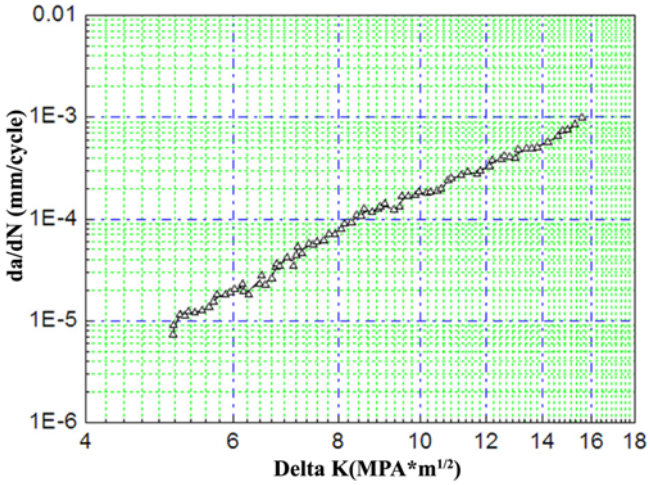

Fig. 3. Fatigue crack propagation rates (da/dN) as a function of the stress intensity factor range (ΔK) of the overaged Al-Zn-Mg-Cu alloy.

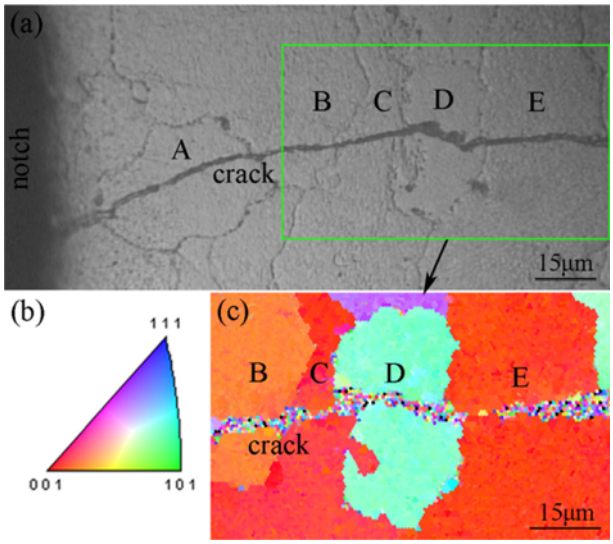

Fig. 4. Optical micrograph (a) and corresponding misorientation distributions (b,c) of the short crack propagation in the near-threshold regime at a ΔK of 4.8 MPa·$m^{1/2}$ (crack propagation from left to right).

Table 3. Misorientation angles and axes of adjacent grains near short crack

Adjacent grains	Misorientation angle (°)	Misorientation axis		
B-C	29.5	0.732144	-0.083657	0.675993
C-D	55.0	0.685586	0.007661	-0.727951
D-E	49.7	0.749284	-0.016089	-0.662054
C-E	7.2	-0.184721	-0.430731	0.883381

4(b) and (c) is responsible for the different misorientations of adjacent grains, in other words, a smaller difference in color indicates a smaller difference in misorientation.

To calculate the misorientations of adjacent grains, the Euler angles of the grains marked B, C, D and E were measured by EBSD, and the misorientation axes and misorientation angles are shown in Table 3. As can be seen, there are dramatic differences in misorientation angles in those grains. Compared with the misorientation angle between grain B and grain C, the misorientation angles between grain E/C and grain D are much higher, reaching 49.7° and 55.0°, respectively, while the difference between grain C and grain E is very small, only 7.2°. Thus, a zigzag crack path forms when the crack passes through grain D, as shown in Figs. 4(a) and (c), due to the great differences in misorientation angles of adjacent grains. At low ΔK values, crack propagation occurs predominantly by single shear in the direction of the primary slip system [14]. Precipitates act as the main barrier against slip and a corresponding stress concentration at the crack tip is released on the slip plane. Therefore, the effect of PFZs on crack propagation is not obvious in this stage.

3.3. Transition of crack propagation path

The transition from the near-threshold regime to the Paris regime of fatigue crack propagation is also accompanied by a noticeable change from short crack to long crack. The morphology of the long crack in the Paris regime is shown in Fig. 5. Figure 5(a) exhibits the misorientation distributions of grains in the Paris regime, which indicates that transgranular crack propagation is dominant. Moreover, a SEM observation of the corresponding long crack was also carried out in order to identify the crack clearly, as shown in Fig. 5(b). Well-defined fatigue striations on the fatigue fracture surface in the Paris regime are illustrated in Fig. 6, and two kinds of grain boundary morphology are observed in Fig. 6(a). The grain boundaries in Fig. 6(a) are highlighted by a blue dashed line, and many tearing grain boundaries are clearly found as arrowed. High-magnification images of the fracture surface shown in Figs. 6(b) and (c) illustrate the characteristics of fatigue striations and grain boundary morphology. The grain boundaries are marked by a dashed line rectangle in Figs. 6(b) and (c).

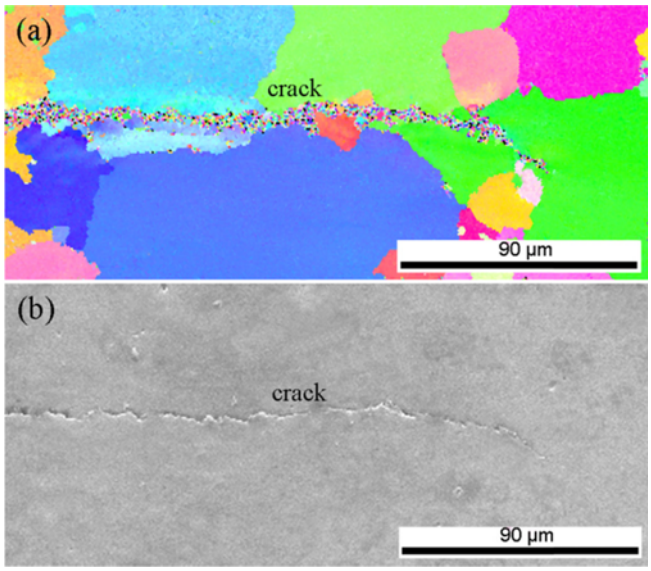

Fig. 5. Transgranular crack propagation is dominant in the Pairs regime at a ΔK of 10 MPa·m$^{1/2}$ (crack propagation from left to right), (a) misorientation distributions of grains, and (b) SEM observation.

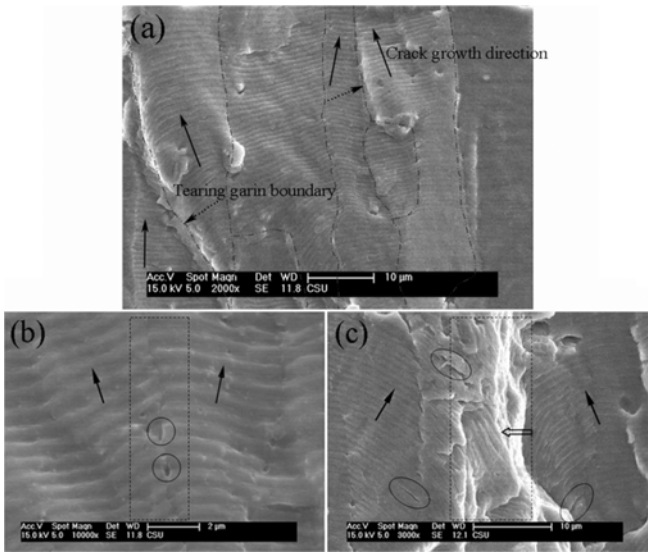

Fig. 6. Fatigue striations and crack propagation planes in adjacent grains in the Paris regime at a ΔK of 10 MPa·m$^{1/2}$, (a) low magnification images, and (b, c) high magnification images.

In Fig. 6(b), cavities form on grain boundary marked by circles owing to the desquamation of GBPs. The fracture surfaces in adjacent grains are shown in Fig. 6(b), suggesting that the cracks in both grains propagate along the same crack plane. The crack is found to propagate vertically along the grain boundary. As a result, the crack propagation path is completely transgranular crack propagation. Different from Fig. 6(b), Fig. 6(c) reveals a discrepancy in the crack propagation plane on adjacent grains. Commonly, a crack propagates along a certain slip plane within each grain until the

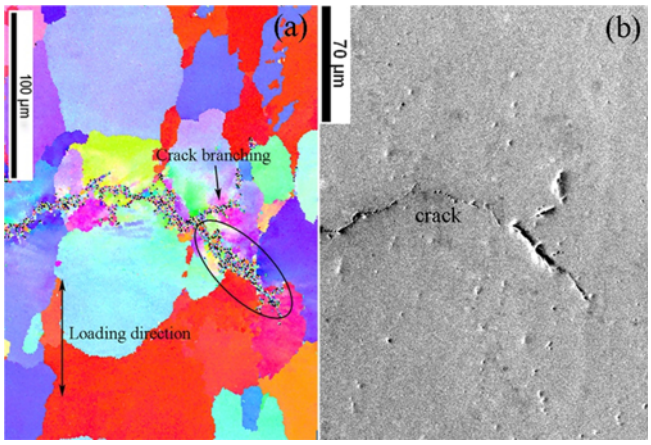

Fig. 7. Intergranular crack propagation and crack branching at the high ΔK (14.9 MPa·m$^{1/2}$) regime, (a) misorientation distributions of grains, and (b) SEM observation.

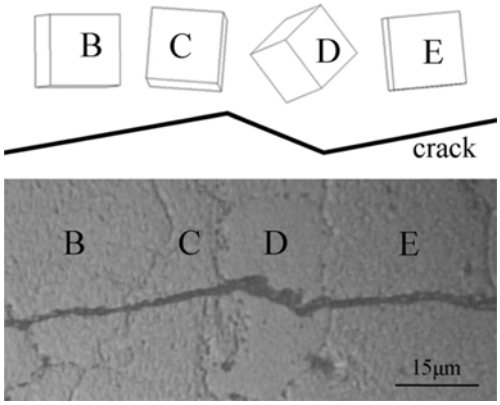

Fig. 8. Schematic illustration of the relationship between misorientation and the crack propagation plane at a ΔK of 4.8 MPa·m$^{1/2}$ (crack propagation from grain B to grain E).

crack impinges on the grain boundary [5,16]. Due to the difference in misorientation of adjacent grains, the crack propagates along different crack planes in each grain as arrowed in Fig. 6(c). As the cracks propagate, a coalescence of crack planes occurs eventually on the grain boundary arising from the presence of PFZs and GBPs. Therefore, the crack propagation path in Fig. 6(c) can be described as partial intergranular crack propagation. Furthermore, fatigue fracture steps on the tearing grain boundary and secondary cracks marked by ellipse near the tearing grain boundary are also observed in Fig. 6(c), indicating the grain boundary is subjected to high stress during cyclic loading at higher ΔK levels.

Figure 7 shows evidence of intergranular crack propagation and transgranular crack branching at high ΔK levels just prior to fatigue fracture. Crack branching is recognized as an acceptable method of retarding crack propagation, since it results in lowering the effective stress intensity and propagation energy at the crack tip. Although the crack branching propagates vertically to the loading direction in Fig. 7, the main crack still tends to propagate along the grain boundary (as marked by ellipse) because the strength of the grain boundary is much weaker than that of the matrix. At high ΔK levels approaching fast fatigue fracture, the crack propagates at an even faster rate, as can be seen in Fig. 3, and the retardation of the FCP rate caused by crack branching can be ignored. Accordingly, despite the presence of crack branching, intergranular crack propagation is predominant at the high ΔK regime.

4. DISCUSSION

According to the studies of Forsyth and Künkler *et al.* [13,14], fatigue crack propagates by different mechanisms at various stages of their evolution. Cracks initiated on active slip bands are referred to as Stage I cracks associated with a single slip mechanism. The crack propagation on a single slip plane is responsible for the formation of a transgranular propagation path. Those mechanisms are well proved in Fig. 4. With further increase in crack length, the crack can be called a "microstructurally short crack". Figure 8 shows the relationship between misorientation and the short crack propagation plane, which indicates zigzag crack forms. In light of the small misorientation between grain B and grain C, as shown in Table 3, there is nearly no change for the crack propagation plane when the crack passes through grains B and C. While the crack impinges on the grain boundary of grain D, deflection occurs because of the high misorientation between grain C and grain D, and the crack propagation plane changes as a consequence. The grain boundary is one of the major barriers to FCP, especially to short crack propagation. The change of crystallographic orientation through a grain boundary results in crack plane deflection [5]. As a result, the transgranular short crack propagation path is greatly influenced by misorientation and the single slip mechanism, whereas the influence of PFZs is limited in this stage.

As Stage I cracks grow larger, they alter the crack path perpendicular to the stress axis, eventually becoming Stage II cracks. Stage II crack propagation, which is conducted by a duplex slip mechanism in the Paris regime, leads to the formation of fatigue striations. As a conceptual models, the Laird model was proposed to explain the growth of stage II cracks and the formation of fatigue striations [17,18]. According to the Laird model, if a grain is loaded along the <100> direction, two {111} planes are symmetrically loaded about the crack plane. Considering that coarse η' precipitates in the overaged alloy are not shearable in nature [19,20], dislocation motion in the slip plane would be impeded. The occurrence of the impeding motion on the primary slip plane leads to alternating shear on another slip plane. Moreover, the irreversibility of cyclic slip causes crack propagation in a planar fashion along the line of the intersection of two slip

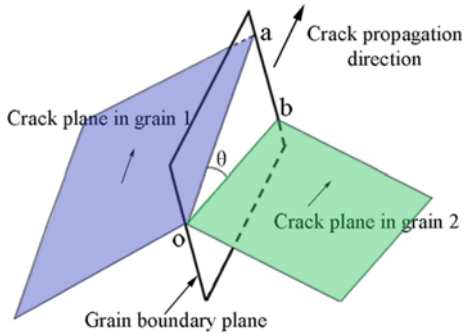

Fig. 9. Schematic diagram showing a crystallographic model of crack propagation.

planes and the formation of fatigue striations on the crack fracture surface. The resulting crack propagation direction is nearly vertical to the intersection line of the two slip planes. Similar phenomena have been observed in the 7075-T6 alloy [16] and 7150-T651 alloy [21], where the crack was found to propagate on {100} planes in the <011> direction. We can deduce, therefore, that crack propagation in the Paris regime is also related to the grain orientation.

In order to fully understand the transition from transgranular to intergranular crack propagation, a crystallographic model is proposed in Fig. 9. One crystallographic parameter of the grain boundary, the tilt angle (θ), is used to account for the intergranular crack propagation path. The tilt angle is the angle between the traces (oa and ob in Fig. 9) of two favored crack planes on the grain boundary plane. Apparently, the magnitude of the θ value represents the extent of intergranular crack propagation on the fatigue fracture surface. θ can be expressed by the following equation,

$$\theta = arcos([E]\times[N_1]\cdot[E]\times[N_2]) \quad (1)$$

where $[E]$, $[N_1]$ and $[N_2]$ are the unit vectors of the grain boundary plane normal and the normal of two crack planes in the adjacent grains, respectively. Based on the analysis mentioned above, therefore, the difference in misorientation of adjacent grains strongly influences the magnitude of the θ value. When the misorientation is small, the transgranular crack propagation path forms as shown in Fig. 6(b). Moreover, the high misorientation results in the intergranular crack propagation as shown in Fig. 6(c). It should be noted that the misorientation is difficult to be identified in practice and this make an exact calculation of the θ value impossible. In addition, at high ΔK levels the sensitivity of crack propagation to microstructure is also very pronounced. In an earlier paper, Xue *et al.* [22] revealed that the distance of fatigue striations changed when the crack passed through the grain boundary in the 7075-T651 alloy without the occurrence of PFZs. Although the grain boundary acts as a barrier of crack propagation, the transgranular crack propagation mode is not changed, just as in the morphology shown in Fig. 6(b). In the case of the overaged alloy in this investigation, when well-defined slip bands impinge on the grain boundary, local stress concentrations are generated from the progressive pileup of dislocations at the end of the slip bands. PFZs will be the preferential site of plastic deformation because of the depletion of solute atoms in the grain boundary area, which offers less resistance to deformation than the matrix reinforced by precipitates. Hence, the local stress concentrations promote the FCP at the grain boundary rather than that in the grain interior. In addition, grain boundaries are particularly effective nucleation sites for equilibrium η precipitates. The response of the GBPs to cyclic deformation results in the easy nucleation of cavities on the interface of GBPs, followed by progressive growth of the cavities with continued deformation and giving rise to their coalescence to form a crack. Therefore, the intergranular crack propagation is aggravated by the presence of GBPs. In conclusion, the transition from transgranular to intergranular crack propagation depends on both the misorientation of adjacent grains and PFZs.

Intergranular crack propagation is also observed in other aluminum alloys. Based on the research on the 2650-T6 alloy [12], the percentage of intergranular crack propagation facets is high in creep-fatigue crack propagation experiments, which was performed at 175 °C with a loading frequency of 0.05 Hz. Fracture surfaces also exhibit significant amounts of intergranular cavity coalescence. Grain boundaries seem to constitute a preferential crack path due to the high concentration of vacancies along these grain boundaries. Therefore, the intergranular cavity coalescence induced by vacancy diffusion control the crack propagation during the creep-fatigue process.

5. CONCLUSIONS

Our study revealed that in the overaged Al-Zn-Mg-Cu alloy, a fatigue crack tends to transgranularly propagate in the near-threshold regime, whereas intergranular crack propagation is dominant at the high ΔK regime. The transition of crack propagation from the transgranular to the intergranular path that occurred in the Paris regime is strongly influenced by the misorientation of adjacent grains and PFZs. Moreover, the formation of a zigzag crack in the near-threshold regime is ascribed to the high misorientation of adjacent grains.

ACKNOWLEDGMENTS

The authors are grateful for the financial support from the National Key Fundamental Research Project of China and the Excellent Doctorate Dissertation Foundation of Central South University.

REFERENCES

1. J. A. Charles, F. A. A. Crane, and J. A. G. Furness, *Selection and Use of Engineering Materials,* 3rd ed., pp. 227-255, Butterworth Heinemann, Oxford (1997).
2. E. A. Starke Jr and J. T. Staley, *Prog. Aerosp. Sci.* **32**, 131 (1996).
3. S. Suresh, A. K. Vasudevan, M. Tosten, and P. R. Howell, *Acta Mater.* **35**, 25 (1987).
4. R. S. Vecchio, R. W. Hertzberg, and R. Jaccard, *Fatigue Fract. Eng. Mater. Struct.* **7**, 181 (1984).
5. T. Zhai, A. J. Wilkinson, and J. W. Martin, *Acta Mater.* **48**, 4917 (2000).
6. T. Zhai, X. P. Jiang, J. X. Li, M. D. Garratt, and G. H. Bray, *Int. J. Fatigue.* **27**, 1202 (2005).
7. Z. Q. Zheng, B. Cai, T. Zhai, and S. C. Li, *Mater. Sci. Eng. A* **528**, 2017 (2011).
8. S. X. Li, R. Q. Chu, J. Y. Hou, and Z. G. Wang, *Philos. Mag. A* **77**, 1081 (1998).
9. H. Zhang, H. Toda, P. C. Qu, Y. Sakaguchi, M. Kobayashi, K. Uesugi, and Y. Suzuki, *Acta Mater.* **57**, 3287 (2009).
10. H. G. Jian, F. Jiang, L. L. Wei, X. Y. Zheng, and K. Wen, *Mater. Sci. Eng. A.* **527**, 5879 (2010).
11. K. S. Chan, *Int. J. Fracture.* **32**, 1428 (2010).
12. G. Hénaff, F. Menan, and G. Odemer, *Eng. Fract. Mech.* **77**, 1975 (2010).
13. P. J. E. Forsyth, *In: Proceedings of Crack Propagation Symposium*, pp.76-94, The College of Aeronautics, Cranfield (1962).
14. B. Künkler, O. Düber, P. Köster, U. Krupp, C.-P. Fritzen, and H.-J. Christ, *Eng. Fract. Mech.* **75**, 715 (2008).
15. S. Suresh, *Fatigue of Materials,* 2nd ed., pp.341-342, Cambridge University Press, Cambridge (1998).
16. C. Q. Bowles and D. Broek, *Int. J. Fracture. Mech.* **8**, 75 (1972).
17. B. Tomkins, *Fatigue Fract. Eng. Mater. Struct.* **19**, 1295 (1996).
18. C. Laird, *ASTM STP.* **415**, 131 (1966).
19. M. N. Desmukh, R. K. Pandey, and A. K. Mukhopadnyay, *Mater. Sci. Eng. A* **435-436**, 318 (2006).
20. B. Sarkar, M. Marek and E. A. Starke Jr, *Metall. Trans. A* **12**, 1939 (1981).
21. A. D. B. Gingell and J. E. King, *Acta Mater.* **45**, 3855 (1997).
22. Y. Xue, H. El Kadiri, M. F. Horstemeyer, J. B. Jordon, and H. Weiland, *Acta Mater.* **55**, 1975 (2007).